NASA
Technical
Paper
2577

March 1986

Pocketing Mechanics of SRM Nozzle Liner

Vincent S. Verderaime

NASA

NASA
Technical
Paper
2577

1986

Pocketing Mechanics of SRM Nozzle Liner

Vincent S. Verderaime

George C. Marshall Space Flight Center
Marshall Space Flight Center, Alabama

National Aeronautics
and Space Administration

**Scientific and Technical
Information Branch**

TABLE OF CONTENTS

LIST OF SYMBOLS

a	Moving coordinate of erosion surface, inch.
b	Liner ring outer radius, inch.
E_p, E_z	Young's modulii in cloth plane and across ply, Msi.
F_c	Composite compression strength, ksi.
F_t	Composite tensile strength, ksi.
h	Depth along liner wall measured radially, inch.
r	Arbitrary radius, inch.
T	Temperature above ambient, °F.
t	Burn time, seconds.
u	Radial displacement, inch.
V_f	Fiber volume fraction, degree.
α_p, α_f	Composite coefficients of thermal expansion, per degree.
ε_r, ε_θ, ε_z	Principal strains.
ν_p, ν_z	Composite Poisson's ratios.
σ_r, σ_θ, σ_z	Principal stresses in cylindrical coordinates, ksi.
ϕ	Fiber fill orientation.

TECHNICAL PAPER

POCKETING MECHANICS OF SRM NOZZLE LINER

I. INTRODUCTION

In the course of a critical failure investigation, it may sometimes be prudent to perform an independent brief analysis in parallel with the more intensive long range team effort. The analysis may be limited in detail, but must be broad in scope and especially capable of rapid manipulation of input variations of environments and properties for a harmonious accounting of a wide range of experiences. Such was the plan of this analysis for the purpose of expediently unfolding events leading to failure scenario and for assessing operational risk periods and significant material parameters requiring further definition.

Over the past dozen Shuttle flights, deep erosion pockets have been observed in Solid Rocket Motor (SRM) nozzle liners and, particularly, on nose rings 403 and 404, Figure 1. They range from shallow wash pockets to 0.9 inch cavities oriented parallel to the combustion gas flow. Erosion at joints have been well characterized as wedge spalls and manufacturing modifications have been prescribed. Mid-length pockets were recognized as fiber rupture in the liner material, but were not completely understood and became the subject of this investigation.

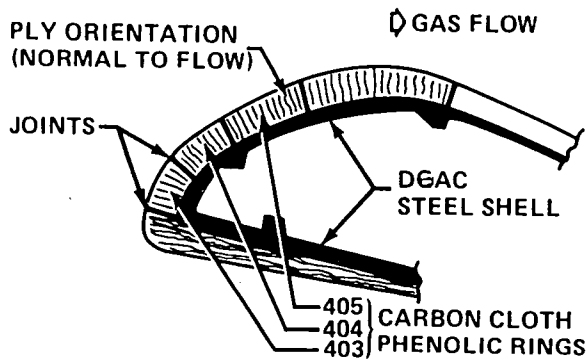

Figure 1. SRM Forward Nozzle Assembly

Special recognition for the outcome of this investigation is due to Dr. George McDonough for initiating and staffing this level of effort, and particularly for his notable insights and suggestions. Acknowledgement is due to Morton-Thiokol Incorporated for providing subject reports and liner material properties data.

II. THERMOELASTIC MODEL

The nozzle liner is constructed of composite rings bonded onto an outer metallic structural shell. The composite is a prepreg phenolic carbon cloth and is plied in planes normal to the gas flow. Dominate loading is caused by the temperature gradient through the liner thickness which is symmetrical about the nozzle axis. The most expedient and explicit formulation of this phenomena was derived from the classical thermoelastic model of a symmetrical cylinder, Figure 2.

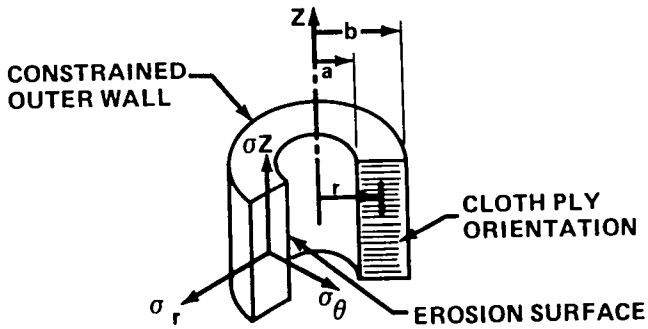

Figure 2. Composite Ring Model

Because of assumed symmetries, shear influences are ignored. Composite properties provided in the fill and warp directions were approximated for the principal stress coordinates in the cloth plane. Both are acceptable compromises in the face of the preliminary status of input data. Due to the high heat flux, the temperature varies over the wall depth (h) with burn time, (t), and, therefore, material properties vary with wall depth and burn time. In addition, the surface at radius (a) recedes as a function of sublimation reaction and erosion and the temperature along the z-axis is uniform.

The equilibrium equation of this two-dimensional model is given by

$$\frac{d\sigma_r}{dr} + \frac{\sigma_r - \sigma_\theta}{r} = 0 \tag{1}$$

and Hook's equations relating to strains induced by stress and thermal expansion are

$$\begin{aligned}
\epsilon_r - \alpha_p T &= (\sigma_r - \nu_p \sigma_\theta)/E_p - \sigma_z \nu_z / E_z \\
\epsilon_\theta - \alpha_p T &= (\sigma_\theta - \nu_p \sigma_r)/E_p - \sigma_z \nu_z / E_z \\
\epsilon_z - \alpha_z T &= \sigma_z/E_z - (\sigma_\theta + \sigma_r)\nu_p/E_p
\end{aligned} \tag{2}$$

Subscript p and z refer to material properties in the cloth plane and normal to it (across ply), respectively.

A major portion of the wall thickness from the outer surface (b) remains at room temperature with correspondingly stiff modulii; therefore, the axial growth and outward radial expansion are assumed restrained and define the boundaries

$$\epsilon_z = 0 \quad \text{and} \quad u = 0 \quad \text{at} \quad r = b \tag{3}$$

Substituting the first condition into equation (2), the principal stresses and strains become

$$\begin{aligned}
\sigma_z &= (\sigma_r + \sigma_\theta)\,\nu_p E_z/E_p - \alpha_z E_z T \\
\epsilon_r - (\alpha_p + \nu_z \alpha_z) T &= \left[\sigma_r - \nu_p \sigma_\theta \left(\frac{1+\nu_z}{1-\nu_p \nu_z}\right)\right](1-\nu_p \nu_z)/E_p \\
\epsilon_\theta - (\alpha_p + \nu_z \alpha_z) T &= \left[\sigma_\theta - \nu_p \sigma_r \left(\frac{1+\nu_z}{1-\nu_p \nu_z}\right)\right](1-\nu_p \nu_z)/E_p \\
\sigma_\theta &= \frac{E_p}{(1-2\nu_p \nu_z)}\,[\epsilon_\theta (1-\nu_p \nu_z) + \nu_p \epsilon_r (1+\nu_z) \\
&\qquad - (1+\nu_p)(\alpha_p + \nu_z \alpha_z) T] \\
\sigma_r &= \frac{E_p}{(1-2\nu_p \nu_z)}\,[\epsilon_r (1-\nu_p \nu_z) + \nu_p \epsilon_\theta (1+\nu_z) \\
&\qquad - (1+\nu_p)(\alpha_p + \nu_z \alpha_z) T]
\end{aligned} \tag{4}$$

Substituting the last two of equations (4) into the equilibrium equation (1) and defining plane strains in terms of radial displacements (u),

$$\epsilon_\theta = \frac{u}{r} \quad \text{and} \quad \epsilon_r = \frac{\partial u}{\partial r} \ , \tag{5}$$

gives

$$\frac{d^2u}{dr^2} + \frac{1}{r}\frac{du}{dr} - \frac{u}{r^2} = \left(\frac{1+\nu_p}{1-\nu_p\nu_z}\right)(\alpha_p + \nu_z\alpha_z)\frac{dT}{dr}$$

which may be written in the form

$$d\left[\frac{1}{r}\frac{d(ur)}{dr}\right] = \left(\frac{1+\nu_p}{1-\nu_p\nu_z}\right)(\alpha_p + \nu_z\alpha_z)\,dT \ .$$

Integrating twice yields the radial displacement,

$$u = \frac{1}{r}\left(\frac{1+\nu_p}{1-\nu_p\nu_z}\right)\int_a^r (\alpha_p + \nu_z\alpha_z)\,T r dr + C_1 r + \frac{C_2}{r} \ , \tag{6}$$

where Poisson's ratios are assumed constant at all temperatures. Strain equations may now be solved in displacement terms by substituting equation (6) into equations (5);

$$\epsilon_\theta = \frac{u}{r} = \frac{1}{r^2}\left(\frac{1+\nu_p}{1-\nu_p\nu_z}\right)\int_a^r (\alpha_p + \nu_z\alpha_z)\,T r dr + C_1 + \frac{C_2}{r^2} \tag{7}$$

$$\epsilon_r = \frac{du}{dr} = -\frac{1}{r^2}\left(\frac{1+\nu_p}{1-\nu_p\nu_z}\right)\int_a^r (\alpha_p + \nu_z\alpha_z)\,T r dr + C_1 - \frac{C_2}{r^2} +$$

$$\left(\frac{1+\nu_p}{1-\nu_p\nu_z}\right)(\alpha_p + \nu_z\alpha_z)\,T \ .$$

Substituting equations (7) into equations (4) will similarly provide a set of stress equations in terms of displacement and integration constants:

$$\sigma_\theta = \left(\frac{1+\nu_p}{1-2\nu_p\nu_z}\right)\left[\frac{1}{r^2}\int_a^r E_p(\alpha_p+\nu_z\alpha_z)\,T r dr - E_p(\alpha_p+\nu_z\alpha_z)\,T + E_p C_1 + E_p\left(\frac{1-\nu_p}{1+\nu_p}\right)\frac{C_2}{r^2}\right]$$

$$\sigma_r = \left(\frac{1+\nu_p}{1-2\nu_p\nu_z}\right)\left[-\frac{1}{r^2}\int_a^r E_p(\alpha_p+\nu_z\alpha_z)\,T r dr + E_p C_1 - E_p\left(\frac{1-\nu_p}{1+\nu_p}\right)\frac{C_2}{r^2}\right] \qquad (8)$$

$$\sigma_z = \left(\frac{1+\nu_p}{1-2\nu_p\nu_z}\right)E_z C_1 - \frac{[\alpha_p(1+\nu_p)+\alpha_z(1+\nu_z)]\,E_z T}{(1-2\nu_p\nu_z)} .$$

Constants of integration are determined by substituting the outer shell constraint of $u = 0$ at $r = b$ into equation (6) and inner condition of $\sigma_r = 0$ at $r = a$ into equation (8) to give

$$C_1 = \left(\frac{1-\nu_p}{1+\nu_p}\right)\frac{C_2}{a^2}$$

$$C_2 = -\frac{(1+\nu_p)^2 a^2}{(1-\nu_p\nu_z)[(1-\nu_p)b^2+(1+\nu_z)a^2]}\int_a^b (\alpha_p+\nu_z\alpha_z)\,T r dr . \qquad (9)$$

III. COMPOSITE MATERIAL PROPERTIES

The above thermoelastic response equations are presented as functions of liner depth between radius "a" and "b". Since the wall temperature gradient increases with time, and varies extensively within these boundaries, then the composite input properties which vary with temperature must necessarily vary with the liner radius. The entire issue of appropriate material engineering constants at elevated temperatures is key to predictions of liner operational conditions. Perhaps the most timely and rewarding approach is to use a common set of existing data [1],

however preliminary, and then adjust the most sensitive and likely property until analytical results match observed liner conditions of recovered nozzles.

The temperature profile, Figure 3, used in this analysis was developed [1] using the conductive heat transfer method which is also based on estimated high temperature properties of the composite. Radiation effects were not included so that the gradient is considered relatively moderate.

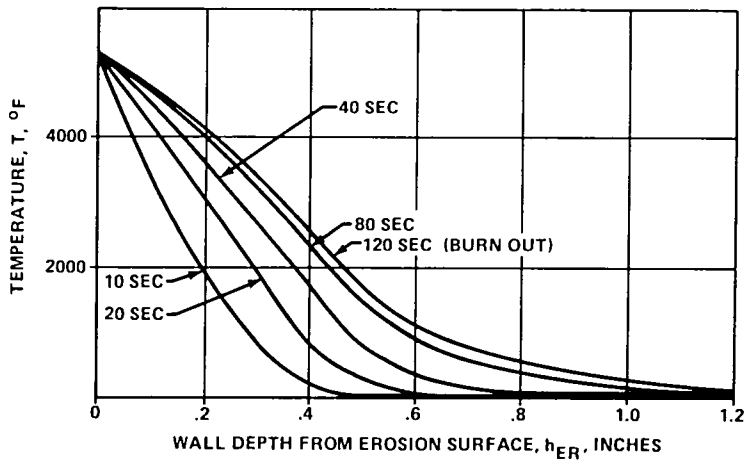

Figure 3. Liner Temperature Gradient

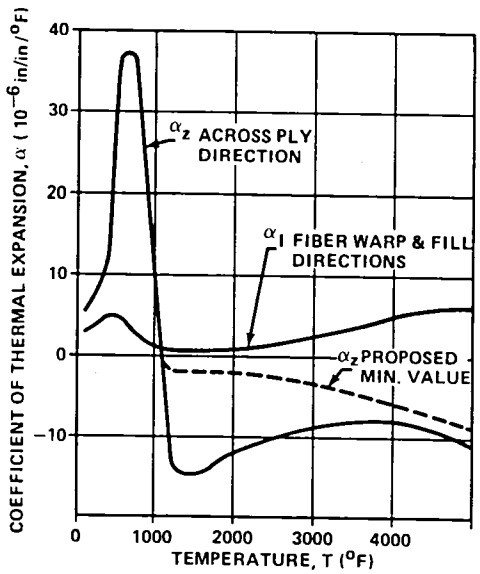

Figure 4. Coefficient of Thermal Expansion

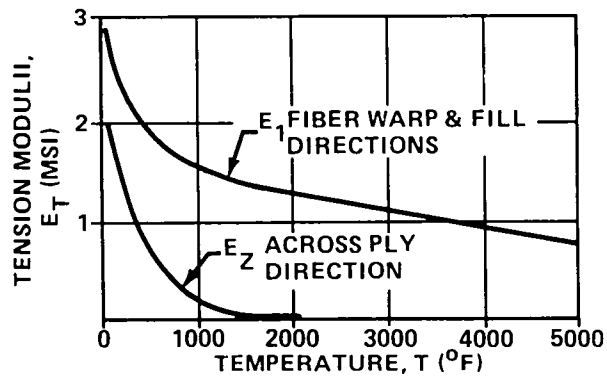

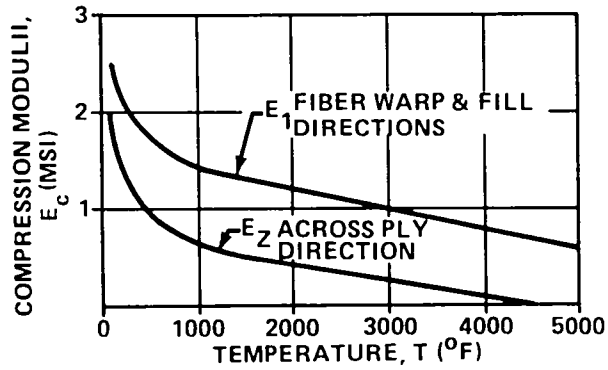

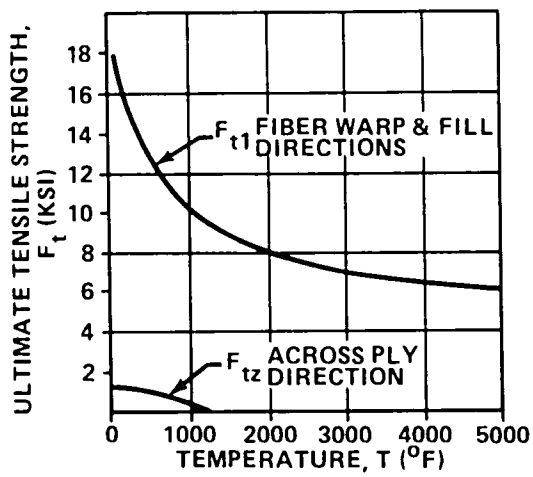

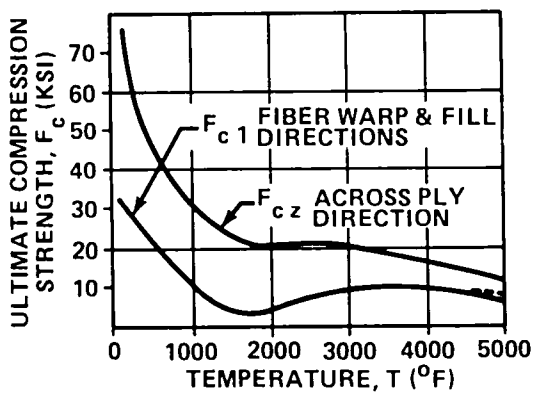

Figure 5. Elastic Properties of Carbon Cloth Phenolic

All of the temperature dependent engineering properties for carbon cloth phenolic are plotted versus the expected temperature range in Figures 4 and 5. Orthotropic material properties along the z-axis (across-ply) are designated by subscript z and those in the warp and fill directions, assumed equal, are designated by subscript 1.

It will be noted in Figure 6 that warp and fill directions in the cloth plane are oriented $\theta = 45°$ from a tangent to the liner wall.

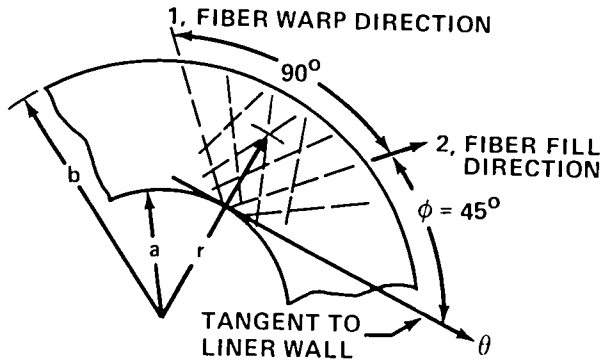

Figure 6. Fiber Fill and Warp Directions in Cloth Plane

To transform the fill and warp oriented experimental properties onto the principal stress and strain axes, coincident with cylindrical coordinates, we need only to know the tensor rank of the engineering properties. Stress, strain and coefficient of thermal expansion are all second rank and may be transformed simply by

$$\begin{Bmatrix} \psi_\theta \\ \psi_r \end{Bmatrix} = \begin{bmatrix} m^2 & n^2 \\ n^2 & m^2 \end{bmatrix} \begin{Bmatrix} \psi_1 \\ \psi_2 \end{Bmatrix}$$

where $m = \cos \phi$ and $n = \sin \phi$. Since $\psi_p = \psi_r$ and $\psi_1 = \psi_2$, then

$$\psi_p = \psi_1 (m^2 + n^2) = \psi_1 \qquad (10)$$

because $m^2 + n^2 = 1$.

This implies that stress, strain and CTE properties are independent of cloth orientation and that subscript p is interchangeable with subscript 1.

Hook's law relation to stiffness is a fourth rank tensor and its transform complexity goes to the heart of micromechanics model involving fiber and resin interaction. However, the most critical part of the pocketing analysis is carried over the charred material, where the interaction between carbon fiber and resin breaks down and lamina cross coupling components vanish. Thus, it can be shown [2] that the fourth rank tensor transform reduces to

$$\begin{Bmatrix} E_\theta \\ E_r \end{Bmatrix} = \begin{bmatrix} m^4 & n^4 \\ n^4 & m^4 \end{bmatrix} \begin{Bmatrix} E_1 \\ E_2 \end{Bmatrix}$$

where $E_p = E_\theta = E_r$ and $E_1 = E_2$. Therefore,

$$E_p = E_1 (m^4 + n^4) = E_1/2 \tag{11}$$

for $\theta = 45°$ and is the least value that may be assumed in principal stress directions.

As usual, Poisson's ratios of composite are difficult to acquire and especially for char conditions. A reasonable estimate for the expected temperature range is

$$\alpha_p = \alpha_1 = .08 \qquad \alpha_z = .26 \tag{12}$$

For convenience, modified properties are incorporated into elastic response equations (7) and (8) and rewritten,

$$\begin{aligned}
\sigma_\theta &= \frac{.56}{r^2} \int_a^r \zeta E_1 \, Tr dr - .56 \zeta E_1 T + .5 K E_1 \left[1 + \left(\frac{a}{r}\right)^2\right] \\
\sigma_r &= \frac{-.56}{r^2} \int_a^r \zeta E_1 Tr dr + .5 K E_1 \left[1 - \left(\frac{a}{r}\right)^2\right] \\
\sigma_z &= 2.2 K E_z - [1.1 \alpha_1 + .77 \alpha_z] \, T E_z \\
\epsilon_\theta &= \frac{1.1}{r^2} \int_a^r \zeta \, Tr dr + K \left[.92 + 1.1 \left(\frac{a}{r}\right)^2\right] \\
\epsilon_r &= \frac{-1.1}{r^2} \int_a^r \zeta \, Tr dr + 1.1 \zeta T + K \left[.92 - 1.1 \left(\frac{a}{r}\right)^2\right]
\end{aligned} \tag{13}$$

where

$$\zeta = (\alpha_1 + .26\,\alpha_z) \qquad \text{and} \qquad K = \frac{-1}{.92\,a^2 + 838} \int_a^b \zeta\, T r dr$$

and the liner initial dimensions are assumed a_o =30 and b = 33 inches.

IV. NOMINAL ELASTIC RESPONSE

Thermoelastic response equations (13) define the stress-strain state of widespread regions and alone cannot explain the localized nature of pockets. Therefore, basic to this investigation is to establish a balance between the response model, engineering properties input and a limiting criterion such as to insure that results represent a nozzle liner that is generally undamaged throughout burn time. Pocketing is assumed to occur from very localized abnominal effects superimposed on nominal response regions.

Response equations are burn time dependent in two respects. One is the moving coordinate, a, which increases with erosion rate and given by

$$a = 30 + .01\,t \text{ inches.} \qquad (14)$$

The other is the changing temperature profile with burn time, over each increment of radius, Δr, from the erosion surface, Figure 3.

To test the compatibility of the elastic model and material properties with observed liner burnout conditions, a burn time of 80 seconds was used because of the deep temperature penetration in a quasi steady state thermal condition. Radial increments of Δr = 0.1 inch seemed adequate for a first cut and the average temperature over each increment was picked from Figure 3. Engineering material properties were selected from Figures 4 and 5 for each average temperature and recorded in columns 2 through 7, Table 1. Elastic response is noted in columns 8 through 10 in the same table.

Because the liner wall thickness to radius is small, the radial stress response was zero for all increments of radius and because of symmetry the tangential strain was negligible and therefore, not recorded. However, those presented revealed essential potential patterns but no clue for visually comparing liner surface with recovered nozzle conditions. A failure criterion was wanted.

TABLE 1

THERMOELASTIC RESPONSE WITH PROPERTIES INPUT

	1	2	3	4	5	6	7	8	9	10	11	12	13
Dep h in.	Temp T °F	CTE α_1	10^{-6} α_z	Mod E_1	MS1 E_z	Strength F_{c1} ksi	F_{cz} ksi	Response σ_θ ksi	σ_z ksi	ϵ_r %	Failure σ_θ	σ_z	ϵ_r
.1	5000	6	-11	.6	0	- 8	-12	-5.3	0	1.7	.9	∞	.7
.2	4400	6	- 9	.7	.1	-10	-15	-6.3	.1	1.8	.6	↓	.8
.3	3600	4	- 8	.9	.2	-11	-19	-3.5	1.2	.7	.3		.4
.4	2800	2	- 9	1.0	.3	-10	-22	.5	3.9	-.1	0.0		-.6
.5	2000	1	-12	1.2	.4	- 5	-21	2.8	6.4	-.5	-.6		-.3
.6	1200	1	-13	1.3	.6	- 7	-28	1.9	6.3	-.3	-.3		-.3
.7	800	2	36	1.5	.7	-14	-36	-7.7	-16.9	1.0	.6	.5	1.0
.8	500	5	22	1.7	.9	-22	-47	-5.2	-10.3	.6	.2	.2	.7
.9	400	5	12	1.8	1.0	-24	-52	-3.4	- 6.1	.3	.1	.1	.4
1.0	200	3	7	2.1	1.5	-30	-70	-1.2	- 2.9	.1	0.0	0.0	.1
1.1	100	3	5	2.5	1.7	-33	-85	- .7	- 1.5	0.0	0.0	0.0	0.0

Clearly, the liner is in a biaxial compression stress state with across ply stress interacting with cloth plane stress. The lack of such biaxial stress test data dispensed with employing the tensor polynomial criterion. Instead, the maximum stress theory,

$$\sigma_i/F_i \geq 1,$$

taken about each axis independently was used with results entered in columns 11 and 12, Table 1.

Since the liner has no tension strength capability across ply direction and above 1000°F, infinity noted in column 12 implies that the liner delaminates from the surface to a 0.6 inch depth without exception. This type failure is not observed on used nozzles. Because only the across ply response is questionable and only above 800° temperature, material inputs were assessed and noted that delamination will always occur when

$$\alpha_z < -1.4\,\alpha_1 \ . \tag{15}$$

The across ply CTE was adjusted accordingly and proposed in Figure 4.

Another failure mode examined was the exceptionally large strain. To be sure, the thermal expansion is directed only in the radial direction and in a tensile strain state, column 10, Table 1. But the corresponding radial stress is zero as discussed earlier! This phenomena is analogous to an isotropic cylinder subjected to uniaxial compression in which the hoop and radial strains progress to a flat disc shape without experiencing hoop and radial stresses. However, in a fiber reinforced matrix, the expansion in the cloth plane is limited by the ultimate strains of the fiber. When the composite is exercised in a thermal environment, as the nozzle liner, then the fiber elastic expansion limit must include a thermal term as proposed in the expression,

$$\epsilon_{f\,ult} = \epsilon_{f\,stress} + \alpha_f T \ . \tag{16}$$

For this investigation, the carbon fiber CTE was assumed constant over the char temperature range, $\alpha_f = 3.8 \times 10^{-6}$ per °F. The fiber elongation was calculated from the uniaxial test relationship

$$\epsilon_{f\,stress} = F_t/E_1 \cong .0065 \tag{17}$$

from 100 to 4000°F. Substitution of these fiber properties into equation (16) gave the appropriate tension strain failure criteria,

$$\epsilon_r/(.0065 + 3.8 \times 10^{-6} T) > 1 \ . \tag{18}$$

When this criterion was imposed on radial strains, fiber failure potentials were noted, Column 13, near the erosion surface and at the .7 inch wall depth. A review of the radial response expression suggested it could be approximated for further examination by

$$\epsilon_r \cong 1.1\,(\alpha_1 + .26\,\alpha_z)\,T \ . \tag{19}$$

It became readily apparent that the potential near the erosion surface was caused by the high temperature. On the other hand, the marginal condition at .7 inch depth was entirely due to the peak across-ply CTE associated with the 800°F experienced at that increment, an obvious parameter to be explored further.

Finally, thermoelastic responses at 80 seconds were recalculated using the proposed across-ply CTE and results presented in Table 2. Again, potential fiber failures were noted near the erosion surface and the 800°F region but no exceedings and no deliminations all of which demonstrated that the modified material properties are nominal and compatible with the thermoelastic model to provide a nominally behaved liner.

MODIFIED

TABLE 2

THERMOELASTIC RESPONSE WITH MODIFIED PROPERTIES

	1	2	3	4	5	6	7	8	9	10	11	12	13
Dep	Temp	CTE	10^{-6}	Mod	MSl	Strength		Response			Failure		
h in.	T °F	α_1	α_z	E_1	E_z	F_{c1} ksi	F_{cz} ksi	σ_θ ksi	σ_z ksi	ε_r %	σ_θ	σ_z	ε_r
.1	5000	6	-9	.6	0	- 8	-12	-6.2	0	2	.8	0	.8
.2	4400	6	-7	.7	.1	-10	-15	-7.3	- .6	2	.7	0	.9
.3	3600	4	-5	.9	.2	-11	-19	-4.9	- .5	1	.5	0	.5
.4	2800	2	-3	1.0	.3	-10	-22	-1.9	0	.3	.2	0	.2
.5	2000	1	-2	1.2	.4	- 5	-21	- .7	.2	.1	.1	0	.1
.6	1200	1	-2	1.3	.6	- 7	-28	-5.2	.1	0	.1	.5	0
.7	800	2	36	1.5	.7	-14	-36	-7.7	-16.9	1	.5	.5	1.0
.8	500	5	22	1.7	.9	-22	-47	-5.2	-10.3	.5	.2	.2	.7
.9	400	5	12	1.8	1.0	-24	-52	-3.3	- 6.2	.3	.1	.1	.4
1.0	200	3	7	2.1	1.5	-30	-70	-1.2	- 3.0	.1	0.0	0.0	.1
1.1	100	3	5	2.5	1.7	-33	-85	- .8	- 1.7	0.0	0.0	0.0	0.0

V. ANALYTICAL METHOD VERIFIED

Balancing a technique to conform with nominal conditions of recovered nozzle liners does beg for credence in the method. An opportunity for verification was recognized in J. R. Koenig's test report [3] on restrained thermal growth (RTG) specimen, Figure 7.

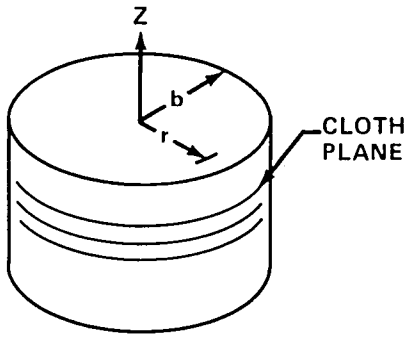

The specimen was a solid cylinder of carbon cloth phenolic with the cloth plane normal to the z-axis. The thermoelastic method developed above was applied with experimental boundaries.

Figure 7. RTG Specimen Coordinates

Specimen was axially restrained, $\epsilon_z = 0$, as was the nozzle ring. Applying the center condition of $u = 0$ at $r = 0$ to equation (6) and letting $a = 0$, one constant was determined to be $c_2 = 0$. Then applying the radial condition of $\sigma_r = 0$ at $r = b$ into the second of equations (8) the other constant was determined

$$C_1 = \frac{1}{b^2} \int_0^b (\alpha_1 + \nu_z \alpha_z)\, T r dr \ . \tag{20}$$

Since the specimen was tested with a uniformly distributed temperature, the coefficient reduced to

$$C_i = (\alpha_1 + \nu_z \alpha_z)\, T/2 \tag{21}$$

and equations (7) and (8) became

$$\begin{aligned} \epsilon_\theta = \epsilon_r &= 1.05\,(\alpha_1 + .26\,\alpha_z)\, T \\ \sigma_z &= -E_z \alpha_z T \end{aligned} \tag{22}$$

for $\nu_1 = .08$ and $\nu = .26$.

To predict the temperature causing fiber rupture, the first of equations (22) was substituted into the failure criterion equation (18). To predict the axial stress corresponding to rupture temperature, the last of equations (22) was employed. Predictions are noted in Table 3.

TABLE 3

RTG FRACTURE PREDICTIONS

Temp	CTE 10^{-6}		Mod	Response		Failure
°F	α_1	α_z	E_z Msi	σ_z ksi	ε_r %	$\varepsilon_r/\varepsilon_f > 1$
1000	1	12	.65	- 8	.4	.4
900	1.5	22	-7.0	-14	.7	.7
800	2.0	36	.7	-20	.9	1.0
700	3.0	37	.75	-19	.9	1.0
600	4.0	36	.8	-17	.8	.9
500	5.0	21	.9	- 9	.5	.6

and imply that the fiber will rupture between 700 and 800°F with a corresponding axial compression load of 20 ksi. Experimental results are summarized in Table 4 and

TABLE 4

RTG COMPOSITE TEST RESULTS [3]

Heating Rate °F/Sec	Fiber Rupture Temp °F	Fiber Rupture Stress Ksi	No. of Specimen
10	734	8.6	17
% COV	± 28	± 36	
30	732	8.7	17
% COV	± 27%	± 20	

temperature prediction is noted to be in very good agreement with the test average. However, the predicted stress is about twice the average tested and implies that the across-ply modulus of the RTG specimen is half that of the SRM nozzle liner.

Since radial and tangential strains are independent of composite modulus, the good agreement of fiber rupture between predicted and test temperatures is sufficient verification of the thermoelastic method and strain failure criterion.

VI. POCKETING PHENOMENA

An engaging output to emerge from the RTG experiment was the large coefficient of variation (COV) in temperature, Table 4, causing fiber rupture. If a set of parameters responsible for large strain variations can be identified, then is it not possible that these parameters are randomly deviated during the liner manufacturing process, and are the cause of localized fissures? If deep pockets are the principal concern, then wouldn't the fiber rupture potential noted at 800°, Table 2, be a case to ponder?

Starting with the approximated radial response equation (19), the sensitivity coefficients of the three material variables at 800°F are

$$\frac{\partial \epsilon_r}{\partial \alpha_1} = 880\,, \quad \frac{\partial \epsilon_r}{\partial \alpha_z} = 230\,, \quad \frac{\partial \epsilon_r}{\partial \nu_z} = .032\,. \tag{23}$$

When these variables were increased, a common percentage, the radial strain increased twelve times more with the across-ply CTE increase than with the other two variables. Then here was a significant parameter, α_z, that might be associated with pocketing, but it was a dependent one. To formulate it into its carbon fiber and phenolic resin constituents, Halp and Pagano's micromechanics model was used,

$$\alpha_z = (1+\nu_m)(1-V_f)\alpha_m + (1+\nu_f)\alpha_f V_f - \alpha_1 (V_f \nu_f + \nu_m (1-V_f)). \tag{24}$$

The nominal fiber volume fraction was assumed, $V_f = 0.6$, and the fiber and resin Poisson's ratios were estimated as

$$\nu_f = .2 \quad \text{and} \quad \nu_m = .45.$$

The composite CTE 's were obtained from Table 2 at 800°F. The resin CTE was found:

$$\alpha_m = 60 \times 10^{-6} \text{ per degree.} \tag{25}$$

Constituent modulii were determined from the rule of mixtures in the fiber direction

$$E_1 = E_m (1-V_f) + E_f V_f \tag{26}$$

and from

$$\alpha_1 E_1 = E_m \alpha_m (1-V_f) + E_f V_f \nu_f$$

where $E_1 = 1.5$ and $\alpha_1 = 2$, Table 2.

Solving simultaneously the resulting modulii

$$E_m = 0 \quad \text{and} \quad E_f = 2.5 \text{ Msi},$$

were substituted into equations (26) to yield $\alpha_1 \simeq \alpha_f$. Having solved each independent variable in equation (24) it was interesting to note that the across ply CTE was independent of the constituent modulii. Furthermore, the only parameter that might be controlled in liner processing is the fiber volume fraction with a sensitivity given by

$$\frac{\partial \alpha_z}{\partial V_f} = \alpha_f (1 - \nu_m) - \alpha_m (1 + \nu_m) = -85 \times 10^{-6} .$$

When this coefficient was combined with the second of equation (23), the desired sensitivity of strain with the across ply CTE independent variable was found

$$\frac{\partial \epsilon_r}{\partial V_f} = \frac{\partial \epsilon_r}{\partial \alpha_z} \cdot \frac{\partial \epsilon_r}{\partial V_f} = -.02 . \qquad (27)$$

Applying this sensitivity to the variational expression,

$$\frac{\Delta \epsilon_r}{\epsilon_r} = \frac{\Delta V_f}{\epsilon_r} \cdot \frac{\partial \epsilon_r}{\partial V_f}$$

the remarkable conclusion was that a 10% increase in resin volume fraction caused a 12% increase in radial strain. It was therefore presumed, that if a high concentration of resin is allowed to flow or pool locally during cure, then an abnormally high across ply CTE will exist to promote localized fiber rupture at the 800°F char region and cause deep pockets.

Another independent liner parameter under intense materials investigation is the carbon fiber strength reduction during processing and cure. The elongation associated with the fiber strength is a significant parameter in the proposed failure criterion, equation (18). It becomes obvious from equation (16) that a 10% reduction in fiber strength translates into a 7% elongation reduction and therefore, reduces the radial straining limit by 7% at 800°F. When this variation and the above resin volume variation occurs separately or in combination, a pocketing scenario is cast.

The scenario begins with the following conditions in place:

1. A region in the liner, Figure 8, has been degraded during processing by an excessive redistribution of resin into a highly concentrated region, a reduction of fiber strength and elongation in a small region, or a combination of both.

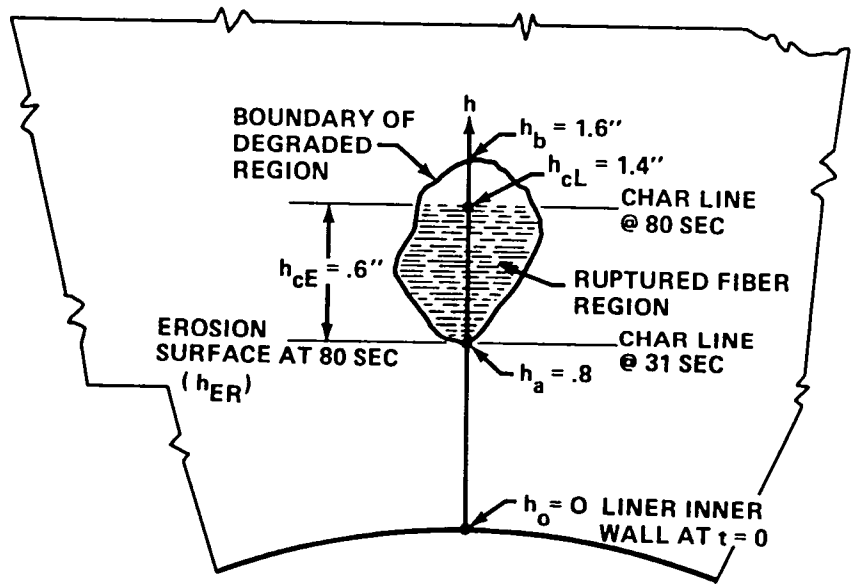

Figure 8. Pocketing Scenario of Degraded Material Region in Cloth Plane

2. Highest potential for fiber rupture occurs when the degraded region is swept by a temperature of approximately 800°, often referred as the char line. This temperature corresponds to the peak value of across ply CTE and penetrates the liner wall at an approximate rate of

$$h_{CE} = [\,(\text{LOG}\, t) - .22\,] \,/\, 2.6 \text{ inches} \qquad (28)$$

from the eroded surface.

3. The liner inner walls recede due to erosion at the rate of

$$h_{ER} = .01 \cdot t \text{ inches.} \tag{29}$$

The total penetration of the char line from the initial inner wall is, therefore, the sum of equations (28) and (29) or

$$h_{CL} = h_{CE} + h_{ER} \cdot \tag{30}$$

As the char line traverses the edge, h_a, of the abnormally processed region, fibers begin to rupture and continue to do so until the char line covers the entire abnormal region or until burn-out. When the liner inner surface erodes to the h_a edge and exposes the ruptured fibers into the gas flow, the disintegrated material is flushed and eroded into pockets in the direction of the gas flow. Using this proposed pocketing model, several time-critical events may be concluded.

Response analysis performed at different burn times similar to Table 2 indicated that high strain potential levels and liner depth are constant. Therefore, no burn time is more favorable to bolstering pocket formation nor depressing it from static strain and pocketing scenario viewpoints. Only the size and location of the degraded region determines the pocket size formed and pocket size observed at burnout.

To demonstrate this, a degraded region was assumed to have a radial dimension of .8 inch ($h_a - h_b$) and with the nearest edge .8 inch (h_a) from liner inner surface. Using equation (30), the char line will begin to traverse the degraded region at 31 seconds and start the fiber rupturing process. It will take the surface erosion process 80 seconds, equation (29), to reach the degraded region at point, h_a, to expose and flush away ruptured fibers. At this time of 80 seconds, the char line will have traveled a distance of 1.4 inches and will have ruptured all the fibers in its path for a total pocket depth of (equation 28) of $h_{ce} = .6$ inches at that burn time. At the same time, a pocket begins to wear in the degraded material region because of the increased erosion rate characteristic of the ruptured material. The temperature gradient in the region is about the same and the pocket depth continues to increase until all the ruptured material is flushed out or until terminated by burnout. In general, no pocketing will occur if the edge h_a of the degraded region is greater than the eroded surface at burn out, 1.2 inches. Pocket depths at burnout decrease as the degraded region edge, h_b, becomes less than the char line travel at burn out, 1.9 inches.

Another, perhaps insidious, condition for deep, narrow pocket formation is that the degraded material region must be ellipsoidally shaped with the longest axis parallel to the liner radial axis. This turns out to be compatible with a manufacturing feature in which the compaction roller axis is parallel with the radial axis. In this orientation, the roller provides the greatest opportunity to create voids with major axis in the radial direction. The voids are presumed to fill with resin which flows into paths and hallows of least resistance during cure and, therefore, produce liner regions of degraded material susceptible to pocketing.

VII. RECOMMENDATIONS

Based upon sensitivity analyses, any processing improvement which inhibits fiber stress (therefore, elongation) reduction or resin concentration will also repress pocket formation. Upgrading specs of fiber cloth strength and resin content for acceptance might also be considered.

Undoubtedly, an FEM analysis will provide a refined basis for strain predictions. However, the classical method used here indicated rather conclusively that strain, and not stress, was the dominant failure mode. Engineering material properties associated with it are rather few and should influence the mechanical properties test programs. A better definition of carbon fiber CTE and elongation over the char temperature range may be required to support the failure criterion. The composite CTE across ply also requires better description over the char temperature range and rate. Resulting values much above 40×10^{-6} per degree must be suspected and test conditions examined for representing char line phenomena existing in the operating nozzle. There is some doubt that material modulii require an improved data base; they are not significant to strain analysis. Same comments apply to composite strengths.

VIII. CONCLUSIONS

A pocketing mechanism was identified in this investigation. It was based on fiber rupture in liner regions which have been degraded during manufacturing process by reducing the fiber strength and allowing resin to flow and concentrate. Failure criterion with a thermal term was proposed.

Pocketing scenario was constructed which noted that only the size and location of the degraded region in the liner determines the size of the pocket formed and the depth observable at burnout.

Materials testing program may be modified to exclude composite modulii and strength since data available is adequate and pocketing is rather insensitive to them. Across ply CTE is the driving input property and should be better defined. This is also true of the fiber CTE and elongation over the char temperature range.

REFERENCES

1. "Structural Verification Analysis for Space Shuttle (SRM) High Performance Motor (HPM) Nozzle Assembly," TWR-14671, April 8, 1985.

2. Mechanics of Composite Materials, McGraw-Hill, R. M. Jones. 1975.

3. JANAF Conference Proceedings, John R. Koenig, Nov. 1984.

1. REPORT NO.	2. GOVERNMENT ACCESSION NO.	3. RECIPIENT'S CATALOG NO.
NASA TP-2577		

4. TITLE AND SUBTITLE	5. REPORT DATE
Pocketing Mechanics of SRM Nozzle Liner	March 1986
	6. PERFORMING ORGANIZATION CODE
7. AUTHOR(S)	8. PERFORMING ORGANIZATION REPORT #
Vincent S. Verderaime	
9. PERFORMING ORGANIZATION NAME AND ADDRESS	10. WORK UNIT NO.
George C. Marshall Space Flight Center Marshall Space Flight Center, Alabama 35812	M-520
	11. CONTRACT OR GRANT NO.
	13. TYPE OF REPORT & PERIOD COVERED
12. SPONSORING AGENCY NAME AND ADDRESS	Technical Paper
National Aeronautics and Space Administration Washington, D. C. 20546	14. SPONSORING AGENCY CODE

15. SUPPLEMENTARY NOTES

Prepared by Systems Dynamics Laboratory, Science and Engineering Directorate.

16. ABSTRACT

A systems approach was adopted to study the pocketing phenomena on a solid rocket nozzle liner. The classical thermoelastic analysis was used to identify marginally strained regions on the composite liner erosion surface and at a depth coincident with the peak value of the across ply coefficient of thermal expansion. A failure criterion was introduced which included a thermal term and permitted failure assessment over the charred liner. The method was verified by satisfactory application to a reported related experiment. Liner pocketing mechanism was attributed to very localized material degradation caused during manufacturing process either by reduction of fiber strength and/or by concentration of resin volume fraction. Pocketing scenario over the degraded material was constructed with supporting formulation to predict size of fissures with respect to degraded material size and location in the liner and with burn time. Sensitivities of liner material parameters were determined to influence test programs designed to update mechanical data base of carbon cloth phenolic over the char temperature range.

17. KEY WORDS	18. DISTRIBUTION STATEMENT
Composites Erosion Liner Erosion Thermoelastic Fracture	Unclassified-Unlimited Subject Category 39

19. SECURITY CLASSIF. (of this report)	20. SECURITY CLASSIF. (of this page)	21. NO. OF PAGES	22. PRICE
Unclassified	Unclassified	25	A02

For sale by National Technical Information Service, Springfield, Virginia 22161

NASA-Langley, 1986